Comput. Methods Appl. Mech. Engrg. 223–224 (2012) 1–9

Contents lists available at SciVerse ScienceDirect

Comput. Methods Appl. Mech. Engrg.

journal homepage: www.elsevier.com/locate/cma

Wave propagation in graphene sheets with nonlocal elastic theory via finite element formulation

B. Arash [a], Q. Wang [a], K.M. Liew [b,*]

[a] Department of Mechanical and Manufacturing Engineering, University of Manitoba, Winnipeg, MB, Canada R3T 5V6
[b] Department of Civil and Architectural Engineering, City University of Hong Kong, Kowloon, Hong Kong Special Administrative Region

ARTICLE INFO

Article history:
Received 27 September 2011
Received in revised form 7 December 2011
Accepted 6 February 2012
Available online 1 March 2012

Keywords:
Graphene sheets
Wave propagation
Nonlocal elasticity
Nonlocal finite element method
Molecular dynamics

ABSTRACT

A nonlocal elastic plate model that accounts for the scale effects is first developed for wave propagations in graphene sheets. Moreover, a finite element model developed from the weak-form of the elastic plate model is reported to fulfill a comprehensive wave study in the sheets and realize an application of the sheets as gas sensors. The applicability of the finite element model is verified by molecular dynamics simulations. The studies show that the nonlocal finite element plate model is indispensable in predicting graphene phonon dispersion relations, especially at wavelengths less than 1 nm, when the small-scale effect becomes dominant. Moreover, the nonlocal parameter e_0a, a key parameter in the nonlocal model, is calibrated through the verification process. The dependence of the small-scale effect and the width of sheets on the dispersion relation is also investigated, and simulation results show that the phase velocity decreases to an asymptotic value with the width of sheets reaches a sufficiently large size. As an application of the investigation, the potential of graphene sheets as nano-sensors for noble gas atoms is explored by defining and examining an index based on the phase velocity shifts in a graphene sheet attached by gas atoms.

1. Introduction

A single-layered graphene sheet (SLGS) is a monolayer of graphite consisting of a repetitive honeycomb lattice in which carbon atoms bond covalently with their neighbors. Since successful fabrications of isolated graphenes [1], graphenes have arisen intense research interests owing to their distinctive and outstanding properties [2], i.e. extremely high elasticity [3] and large thermal conductivity [4]. These properties have made graphene sheets (GSs) as one of the most promising materials for wide potential applications in nanotechnology [5–8], such as gas detection, graphene transistors, solar cells, and diagnosis devices.

Recently, interests have been generated in the area of terahertz physics of nanoscale materials and devices [9–12] which opens a new topic on nano-materials wave characteristics. Chen et al. [10] provided a potentially useful mechanism for using a single-walled carbon nanotube (SWCNT) as a vehicle to deliver large drug molecules. Their simulations showed that the transport and ejection of molecules via a SWCNT can be achieved by mechanical wave propagation in the SWCNT. The formation of ripples in a graphene sheet (GS) when it is stroked by a C60 molecule was recently investigated [11]. It was indicated that the ripple propagation in a graphene can be used to detect defects in the SLGS. The potential of a GS-based sensor in detection of gas atoms via a vibration analysis was proposed as well [12] and an index based on frequency shift of a GS induced attached by gas atoms on its surface was presented.

Potential applications of nano-materials depend on a thorough understanding of their mechanical properties and behaviors through modeling and experimental investigations. In addition to experimental works, there are three main approaches for theoretical modeling of nanostructures: (a) atomistic modeling, (b) hybrid atomistic–continuum mechanics and (c) continuum mechanics. Atomic modeling includes techniques such as classical molecular dynamics (MD), tight-binding molecular dynamics (TBMD) and the density functional theory (DFT) [13–16]. These atomic methods are limited to systems with a small number of molecules and atoms. Hybrid atomistic–continuum mechanics allows one to directly incorporate interatomic potential into the continuum analysis [17,18]. Continuum mechanics includes classical (or local) beam, plate and shell theories that are practical for analyzing large-scale nano-systems (or nano-systems) [19–21]. Continuum mechanics approach is less computationally expensive than the former two approaches and their formulations are relatively simple. Although classical or local continuum modeling is effective in studying large-scale nanostructures, its applicability to identify the small-scale effect on nano-material mechanical behaviors is limited. The limited applicability is due to the fact that at small size

* Corresponding author. Tel.: +852 3442 7601; fax: +852 3442 0427.
E-mail address: kmliew@cityu.edu.hk (K.M. Liew).

0045-7825/$ - see front matter © 2012 Elsevier B.V. All rights reserved.
doi:10.1016/j.cma.2012.02.002

the lattice spacing between individual atoms becomes increasingly important and the discrete structure of the material can no longer be homogenized into a continuum. Therefore, cautious employment of classical continuum models has been proclaimed when directly applying to nanostructure analysis [22–24]. The essence of the nonlocal elasticity theory developed by Eringen [25,26], on the other hand, indicates that the stress state at a given reference point is a function of the strain field at every point in the body, and hence the theory could account for information about the long range forces between atoms and the scale effect. Wang [27] investigated wave propagation in CNTs with the nonlocal elastic Euler–Bernoulli and Timoshenko beam models. Flexural wave propagation in SWCNTs was investigated for a wide range of wave numbers by the nonlocal beam models and MD simulations [28]. It was indicated that the nonlocal shell theory is indispensable in predicting carbon nanotube (CNT) phonon dispersion relations at small wavelengths [29]. Hu et al. [30] modeled SWCNTs and double-walled CNTs (DWCNTs) by nonlocal single and double elastic cylindrical shells. It was indicated that the wave dispersion predicted by the nonlocal elastic cylindrical shell theory is in good agreement with that with MD simulations in a wide frequency range up to the terahertz region. Wave propagation in GSs was studied in Refs. [31–35]. Narendar et al. [32] investigated the small-scale effect on wave dispersion characteristics of SLGSs using nonlocal continuum theory. However, since only continuum mechanics was employed in these studies, no calibration on the scale parameters used in the nonlocal theories was conducted in theses references, and the applicability of the nonlocal theories was not justified. A literature survey also shows that the application of the nonlocal finite element (FE) method in studying wave propagation in sheets has not been investigated in previous studies.

This paper aims to provide a comprehensive study on wave propagations in SLGSs by a developed nonlocal finite element plate model and MD simulations. The effect of the size of the sheet width on GS phonon dispersion relations is studied and the nonlocal parameter is calibrated for a range of wavenumbers through the verification process. The potential of GSs in design of nano-sensors that are able to fulfill a detection purpose of atoms or molecules is investigated as a byproduct of the wave analysis.

2. Nonlocal finite element plate model

According to the nonlocal theory by Eringen [25,26], the stress at a reference point x in an elastic continuum not only depends on the strain at the point but also on strains at every point of the body. This is attributed by Eringen to the atomic theory of lattice dynamics and experimental observations on phonon dispersion. The basic equations for linear homogenous and isotropic elastic solids neglecting the body forces are

$$\begin{aligned} &\sigma_{ij,j} = 0, \\ &\sigma_{ij}(x) = \int \lambda(|x-x'|,\alpha) C_{ijkl}\varepsilon_{kl}(x')dV(x'), \quad \forall x \in V, \\ &\varepsilon_{ij} = \frac{1}{2}(u_{i,j}+u_{j,i}), \end{aligned} \tag{1}$$

where σ_{ij} and ε_{ij} are the stress and strain tensors, respectively; C_{ijkl} is the elastic modulus tensor in classical isotropic elasticity; and u_i is the displacement vector. Eq. (1) shows that stress (σ) at a reference point depends on a local strain at the source x' induced within a finite volume, V, surrounding the material point, by means of a nonlocal kernel $\lambda(|x-x'|,\alpha)$ that weights the classical strains around point x. λ is the nonlocal modulus or attenuation function which is a function of the distance in Euclidean form, $|x-x'|$, and a material constant α. Material constant α defined as e_0a/l depends on the internal characteristics lengths, a (lattice parameter, granular size, distance between C—C bonds), external characteristics lengths l (crack length, wave length) and e_0a is the scale coefficient or nonlocal parameter revealing the small-scale effect on the responses of nano-structures. Generally, in analysis of CNTs the nonlocal scale coefficients e_0a are taken in the range 0–2 nm [27]. The kernel function $\lambda(|x-x'|,\alpha)$ is given by Eringen as

$$\lambda(|x|,\alpha) = (2\pi l^2\alpha^2)^{-1}K_0\left(\frac{\sqrt{x.x}}{l\alpha}\right), \tag{2}$$

where K_0 is the modified Bessel function. The constitutive relation may be obtained as follows based on Eqs. (1) and (2)

$$(1-(e_0a)^2\nabla^2)\sigma = C:\varepsilon, \tag{3}$$

where $\nabla^2 = \left(\frac{\partial}{\partial x^2}+\frac{\partial}{\partial y^2}\right)$ is the Laplacian operator. In classic plate theory, transverse shear strains are neglected. The dynamic equilibrium equation of a nano-plate in terms of the displacements is given as [21]

$$-D\nabla^4 w = (1-(e_0a)^2\nabla^2)\left[I_0\frac{\partial^2 w}{\partial t^2} - I_2\left(\frac{\partial^4 w}{\partial x^2\partial t^2}+\frac{\partial^4 w}{\partial y^2\partial t^2}\right)\right], \tag{4}$$

where D is the bending rigidity; $I_0 = \rho h$ and $I_2 = \frac{1}{12}\rho h^3$ are respectively the first and second mass moments of inertia; ρ is the mass density. It is noted that the local field equations are recovered when the nonlocal parameter (e_0a) is set to zero.

The wave propagation solution for GSs can be expressed as

$$w(x,y,t) = We^{i(lx+ky-\omega t)}, \tag{5}$$

where W denotes the transverse displacement amplitude of sheets; l and k are respectively the wavenumber in x- and y-directions; ω is the frequency of the wave motion. For waves in y-direction the wavenumber in y-direction, $l = 0$ is set. Substituting Eq. (5) into Eq. (4) gives the phase velocity

$$c = \frac{\omega}{k} = k\sqrt{\frac{D}{\rho h(1+(e_0a)^2k^2)}}. \tag{6}$$

Eq. (6) indicates that the small-scale effect on wave propagation in a GS decreases the phase velocity. For example, the phase velocity in the GS decreases from 2.76×10^3 m/s for $e_0a = 0$ to 2.35×10^3 m/s for $e_0a = 0.18$ nm at a harmonic deflection of period $T = 500$ fs (or an angular frequency of $\omega = \frac{2\pi}{T} = 1.26\times10^{13}$ rad/s).

In the research, a GS is approximated to be a plate structure using the classic plate theory in cooperation with the nonlocal continuum theory. Due to the fact that many intrinsic ripples are observed in a GS [36], fixed boundary conditions are considered at edges of the GS in its width direction to stiffen the sheet to ensure propagation of waves in the graphene.

Although Eq. (6) is obtained to provide an explicit wave dispersion relation between the phase velocity and wavenumber of a GS, two limitations come from the theoretical elastic plate model: (1) the effects of the width length of the sheet and fixed edges in its width direction to stiffen the sheet to ensure propagation of waves in the GS cannot be modeled in the theoretical model, and (2) potential applications of GSs as nano-sensors in detection of gas atoms on their surfaces via a wave propagation analysis cannot be conducted by the simple theoretical model as some physical complexities cannot be interpreted or described with the simple model, such as the distribution of external gases on sheet surfaces. To compromise the limitations of the theoretical model, a nonlocal FE plate model is developed in the study. By this FE model, the effects of the width length and fixed boundary conditions of GSs can all be accounted. Furthermore, a GS as nano-sensors with gas atoms on its surface can be modeled as a plate structure with nonuniform mass

density by the nonlocal finite element plate model. It should be noted that since the shear effect and rotary inertia are not considered in the classical model, the wave solution for higher wavenumbers could not be predicted efficiently by the model.

To develop the finite element model, a weak form of Eq. (4) is first provided by multiplying by a weight function δu and integrating the equation over the element domain Ω_e [31],

$$\int_{\Omega_e} \delta u \left\{ D\nabla^4 w + (1-(e_0a)^2\nabla^2)\left[I_0 \frac{\partial^2 w}{\partial t^2} - I_2\left(\frac{\partial^4 w}{\partial x^2 \partial t^2} + \frac{\partial^4 w}{\partial y^2 \partial t^2} \right) \right] \right\} dxdy = 0. \tag{7}$$

To reduce the differentiability of the interpolation functions used in the FE approximation of w, differentiations on Eq. (7) are integrated by part as

$$\begin{aligned}
&\int_{\Omega_e} (\delta u_{,xx} w_{,xx} + 2\delta u_{,xy} w_{,xy} + \delta u_{,yy} w_{,yy}) dxdy \\
&+ \int_{\Omega_e} (I_0 \delta u w_{,tt} + I_2(\delta u_{,x} w_{,xtt} + \delta u_{,y} w_{,ytt})) dxdy \\
&+ (e_0a)^2 \int_{\Omega_e} (I_0(\delta u_{,x} w_{,xtt} + \delta u_{,y} w_{,ytt}) + I_2(\delta u_{,xx} w_{,xxtt} \\
&+ 2\delta u_{,xy} w_{,xytt} + \delta u_{,yy} w_{,yytt})) dxdy \\
&+ \int_{\Gamma_e} (\delta u w_{,xxx} n_x - \delta u_{,x} w_{,xx} n_x + 2\delta u w_{,xyy} n_x - 2\delta u_{,x} w_{,xy} n_y \\
&+ \delta u w_{,yyy} n_y - \delta u_{,y} w_{,yy} n_y) ds, \\
&- \int_{\Gamma_e} (I_2 + (e_0a)^2 I_0)(\delta u w_{,xtt} n_x + \delta u w_{,ytt} n_y) \\
&+ (e_0a)^2 \int_{\Gamma_e} I_2((\delta u w_{,xxtt} - \delta u_{,x} w_{,xtt})(n_x + n_y) \\
&+ 2\delta u w_{,xytt} n_x + 2\delta u_{,x} w_{,xytt} n_y) = 0,
\end{aligned} \tag{8}$$

where x, y and t in subscripts denote derivatives respect to x, y and t. (n_x, n_y) are the direction cosines of the unit normal on the boundary Γ_e of the element domain Ω_e. The approximation displacement $w = \sum_j X_j \phi_j(x,y)$ $(j = 1-16)$ is applied over an element by Hermite interpolation functions, ϕ_j, where X_j denotes nodal values of w and its derivatives. The Hermite cubic interpolation of $w, \frac{\partial w}{\partial x}, \frac{\partial w}{\partial y}$, and $\frac{\partial^2 w}{\partial x \partial y}$ using four-node rectangular elements plotted in Fig. 1 is provided as follows [37],

$$\begin{array}{l}
\frac{1}{16}(\xi+\xi_i)^2(\xi\xi_i-2)(\eta+\eta_i)^2(\eta\eta_i-2), \ \textit{Variable } w \\
-\frac{1}{16}\xi_i(\xi+\xi_i)^2(\xi\xi_i-1)(\eta+\eta_i)^2(\eta\eta_i-2), \ \textit{Variable} \frac{\partial w}{\partial \xi} \\
-\frac{1}{16}(\xi+\xi_i)^2(\xi\xi_i-2)\eta_i(\eta+\eta_i)^2(\eta\eta_i-1), \ \textit{Variable } \frac{\partial w}{\partial \eta} \\
\frac{1}{16}\xi_i(\xi+\xi_i)^2(\xi\xi_i-1)\eta_i(\eta+\eta_i)^2(\eta\eta_i-1), \ \textit{Variable } \frac{\partial^2 w}{\partial \xi \partial \eta}
\end{array} \quad \text{for node } i(i=1,\ldots,4), \tag{9}$$

where ξ and η denote natural coordinates of the Hermit cubic element shown in Fig. 1. The finite expression of the nonlocal FE model based on the weak form of Eq. (8) and the Hermite cubic interpolation shown in Eq. (10) can be expressed in a matrix form for an element as

$$[M^e]\{\ddot{X}^e\} + [K^e]\{X^e\} = 0, \tag{10}$$

where

$$[K^e] = \int_{\Omega_e} [B^e]^T \begin{bmatrix} D & 0 & 0 \\ 0 & 2D & 0 \\ 0 & 0 & 0 \end{bmatrix} [B^e] dxdy,$$

$$[B^e] = \begin{bmatrix} \phi_{1,xx} & \phi_{2,xx} & \phi_{3,xx} & \phi_{4,xx} & \phi_{5,xx} & \phi_{6,xx} & \phi_{7,xx} & \phi_{8,xx} & \phi_{9,xx} & \phi_{10,xx} & \phi_{11,xx} & \phi_{12,xx} & \phi_{13,xx} & \phi_{14,xx} & \phi_{15,xx} & \phi_{16,xx} \\ \phi_{1,xy} & \phi_{2,xy} & \phi_{3,xy} & \phi_{4,xy} & \phi_{5,xy} & \phi_{6,xy} & \phi_{7,xy} & \phi_{8,xy} & \phi_{9,xy} & \phi_{10,xy} & \phi_{11,xy} & \phi_{12,xy} & \phi_{13,xy} & \phi_{14,xy} & \phi_{15,xy} & \phi_{16,xy} \\ \phi_{1,yy} & \phi_{2,yy} & \phi_{3,yy} & \phi_{4,yy} & \phi_{5,yy} & \phi_{6,yy} & \phi_{7,yy} & \phi_{8,yy} & \phi_{9,yy} & \phi_{10,yy} & \phi_{11,yy} & \phi_{12,yy} & \phi_{13,yy} & \phi_{14,yy} & \phi_{15,yy} & \phi_{16,yy} \end{bmatrix};$$

and $[M^e] = [M^e_L] + [M^e_{NL}]$, $[M^e_L] = \int_{\Omega_e} \left([N^e]^T I_0 [N^e] + [N^e_x]^T \begin{bmatrix} I_2 & 0 \\ 0 & I_2 \end{bmatrix} [N^e_x] \right) dxdy$,

$$[M^e_{NL}] = \int_{\Omega_e} (e_0a)^2 [[N^e_x]^T \begin{bmatrix} I_0 & 0 \\ 0 & I_0 \end{bmatrix} [N^e_x] + [N^e_{xx}]^T \begin{bmatrix} I_2 & 0 & 0 \\ 0 & 2I_2 & 0 \\ 0 & 0 & I_2 \end{bmatrix} [N^e_{xx}]] dxdy,$$

the term that accounts for the nonlocal effect in graphene sheets,

$$[N^e] = [\phi_1\ \phi_2\ \phi_3\ \phi_4\ \phi_5\ \phi_6\ \phi_7\ \phi_8\ \phi_9\ \phi_{10}\ \phi_{11}\ \phi_{12}\ \phi_{13}\ \phi_{14}\ \phi_{15}\ \phi_{16}],$$

$$[N^e_x] = \begin{bmatrix} \phi_{1,x} & \phi_{2,x} & \phi_{3,x} & \phi_{4,x} & \phi_{5,x} & \phi_{6,x} & \phi_{7,x} & \phi_{8,x} & \phi_{9,x} & \phi_{10,x} & \phi_{11,x} & \phi_{12,x} & \phi_{13,x} & \phi_{14,x} & \phi_{15,x} & \phi_{16,x} \\ \phi_{1,y} & \phi_{2,y} & \phi_{3,y} & \phi_{4,y} & \phi_{5,y} & \phi_{6,y} & \phi_{7,y} & \phi_{8,y} & \phi_{9,y} & \phi_{10,y} & \phi_{11,y} & \phi_{12,y} & \phi_{13,y} & \phi_{14,y} & \phi_{15,y} & \phi_{16,y} \end{bmatrix},$$

$$[N^e_{xx}] = \begin{bmatrix} \phi_{1,xx} & \phi_{2,xx} & \phi_{3,xx} & \phi_{4,xx} & \phi_{5,xx} & \phi_{6,xx} & \phi_{7,xx} & \phi_{8,xx} & \phi_{9,xx} & \phi_{10,xx} & \phi_{11,xx} & \phi_{12,xx} & \phi_{13,xx} & \phi_{14,xx} & \phi_{15,xx} & \phi_{16,xx} \\ \phi_{1,xy} & \phi_{2,xy} & \phi_{3,xy} & \phi_{4,xy} & \phi_{5,xy} & \phi_{6,xy} & \phi_{7,xy} & \phi_{8,xy} & \phi_{9,xy} & \phi_{10,xy} & \phi_{11,xy} & \phi_{12,xy} & \phi_{13,xy} & \phi_{14,xy} & \phi_{15,xy} & \phi_{16,xy} \\ \phi_{1,yy} & \phi_{2,yy} & \phi_{3,yy} & \phi_{4,yy} & \phi_{5,yy} & \phi_{6,yy} & \phi_{7,yy} & \phi_{8,yy} & \phi_{9,yy} & \phi_{10,yy} & \phi_{11,yy} & \phi_{12,yy} & \phi_{13,yy} & \phi_{14,yy} & \phi_{15,yy} & \phi_{16,yy} \end{bmatrix}.$$

Assembling the element matrices into the global matrix gives the nonlocal FE model,

$$[M]\{\ddot{X}\} + [K]\{X\} = 0, \tag{11}$$

The Houbolt integration scheme [38] is used to solve the dynamic Eq. (12). The Houbolt integration scheme is a step-by-step

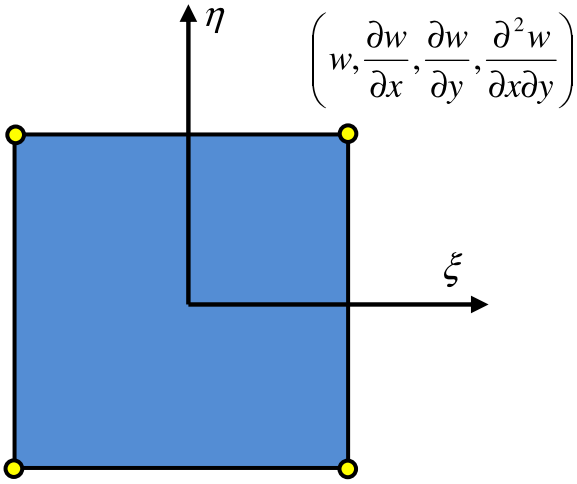

Fig. 1. Schematic of a Hermit cubic element.

solution scheme based on standard finite difference expressions to approximate the acceleration components in terms of the displacement components.

Modeling of an application of GSs as nano-sensors can be realized from the above nonlocal FE modeling. In the application, gas atoms attached on the sheet surfaces can be treated with a non-uniform mass density in the mass matrix with the nonlocal FE plate model. The mass density of a mesh without and with a gas atom on its surface is respectively assumed to be ρ and $\rho_{mass} = \rho + \frac{m_{atom}}{A_e h_e}$ where m_{atom}, A_e and h_e are mass of the gas atom on the mesh, area of the mesh, and thickness of the mesh, respectively. The locations of atoms are randomly located on graphenes in the FE model.

3. Molecular dynamics simulations

Molecular dynamics is a powerful method to analyze nanoscale systems by solving Newtonian equations of motion governed by interatomic interactions to numerically determine the trajectories of a large number of atoms. For the interaction potential, the second-generation reactive empirical bond order (REBO) potential energy expression for hydrocarbons developed by Brenner et al. [39] is adopted to simulation wave propagations in GSs. In the second-generation REBO potential, the total potential energy of a system is given by

$$E_{REBO} = \sum_i \sum_{j=i+1} [E_R(r_{ij}) - \bar{b}_{ij} E_A(r_{ij})], \tag{12}$$

where r_{ij} is the distance between the pairs of adjacent atoms i and j, and $\bar{b}_{ij}$ is a many-bond empirical bond-order term. The *vdW* interactions between a GS and external atoms attached on the GS are modeled by the Lennard–Jones potential [40],

Table 1
Atomic mass, well-depth energy (ε), and the equilibrium distance (σ) of C, Ne, Ar, Kr and Xe atoms taken from Ref. [41].

Type of atom	Atomic mass (amu)	ε/K_b(K)[a]	σ (nm)
Carbon (C)	12.011	51.2	0.335
Neon (Ne)	20.179	47	0.272
Argon (Ar)	39.948	119	0.341
Krypton (Kr)	83. 798	164	0.383
Xenon (Xe)	131.293	224.5	0.407

[a] K_b is Boltzmann's constant.

$$V_{ij}(r_{ij}) = 4\varepsilon \left[\left(\frac{\sigma}{r_{ij}}\right)^{12} - \left(\frac{\sigma}{r_{ij}}\right)^{6} \right], \tag{13}$$

where ε and σ are respectively the coefficients of well-depth energy and the equilibrium distance. For carbon atoms in a GS and the attached noble gas atoms, the coefficients can be approximated using the venerable Lorentz–Berthelot mixing rules [41] as

$$\sigma_{AB} = \frac{1}{2}(\sigma_{AA} + \sigma_{BB}), \quad \varepsilon_{AB} = \sqrt{\varepsilon_{AA}\varepsilon_{BB}}. \tag{14}$$

The noble gases, i.e. Neon (Ne), Argon (Ar), Krypton (Kr) and Xeon (Xe), are considered as atoms on surface of a GS which interact with the GS through the vdW interactions. The coefficients of well-depth energy, ε, and the equilibrium distance, σ, used in Eqs. (13) and (14) taken from Ref. [41] are provided in Table 1 for each type of atoms. A minimization process of energy is conducted to model an equilibrium state of the GS with noble gas atoms on its surface. After the minimization process of energy, noble gas atoms are found to be distributed on the GS and their distribution is found to be in a random way on the GS in equilibrium distance defined in Eq. (15). A Velocity-Verlet algorithm is used to integrate the equations of motion and an incremental time step is set to be 1 fs. The Nose–Hoover feedback thermostat [42] is employed for system temperature conversion at 300 K. The histories of the geometric centric atoms of two arbitrary sections of a GS are recorded for a certain duration (5–10 ps depending on the harmonic deflection of period), and then the wavenumber and the phase velocity are computed.

4. Results and discussion

The material parameters of GSs used in the following simulations are taken from Ref. [30] and the in-plane stiffness $Eh = 360\ \mathrm{J/m^2}$, the mass density $\rho = 2.27\ \mathrm{g/cm^3}$ and the effective thickness $h = 0.34$ nm are set. The bending rigidity $D = 1.78$ ev proposed by Wang and Liew [43] for relatively large nano-tubes and GSs is employed in this study.

First, to investigate the applicability of the nonlocal FE model in predicting the wavenumber and the phase velocity of GSs, the wave dispersion relations of a square SLGS with a size of 15 nm and the nonlocal parameter of $e_0 a = 18$ nm based on the nonlocal FE model with a number of elements of 6×50 are compared with those based on the theoretical elastic plate model presented in Eq. (6), and the results are shown in Table 2. In the comparison, the GS is subjected to harmonic deflection of period ranging from 200 fs to 1000 fs at $y = 0$ as shown in Fig. 2. The numerical results obtained are found to be in great agreement with ones from the theoretical elastic plate model with a percentage difference only about 0.1% and the convergence of the nonlocal FE model is satisfied with the element mesh.

A snapshot of wave propagating in y direction of an armchair GS with a width of 3.62 nm and a length of 15.03 nm subjected to a harmonic deflection of period $T = 500$ fs at $y = 0$ by both the continuum model and MD simulations is presented in Fig. 2(a) and (b). Two layers of carbon atoms are fixed at graphene edges to decrease the influence of the intrinsic ripples to ensure propagation of waves in the sheet. In the following simulations, sheets with the same sizes in Fig. 2 are considered, otherwise is mentioned.

The phase velocity and wave number can be determined from the signals of the transverse vibrations of atoms in two arbitrary sections of the GS. In simulations, one atomic layer located in section 0 at $y = 0$ of the GS shown in Fig. 2 is subjected to a harmonic deflection of period $T = 500$ fs and is shown in Fig. 3(a). Fig. 3(b)

Table 2
Comparison the wavenumber and the phase velocity obtained by the nonlocal FEM model with the nonlocal theoretical elastic model with a nonlocal parameter of e_0a = 0.18 nm for a SLGS with the size of 15 × 15 nm.

Harmonic deflection of period (fs)	Theoretical elastic plate model		FEM model[a]	
	Wavenumber ($\times 10^9$ l/m)	Phase velocity ($\times 10^3$ m/s)	Wavenumber ($\times 10^9$ l/m)	Phase velocity ($\times 10^3$ m/s)
200	10.052	2.986	1.051	2.989
400	6.232	2.521	6.228	2.522
600	4.764	2.198	4.762	2.199
800	3.988	1.969	3.985	1.971
1000	3.494	1.797	3.493	1.799

[a] Number of elements taken is 6 × 50.

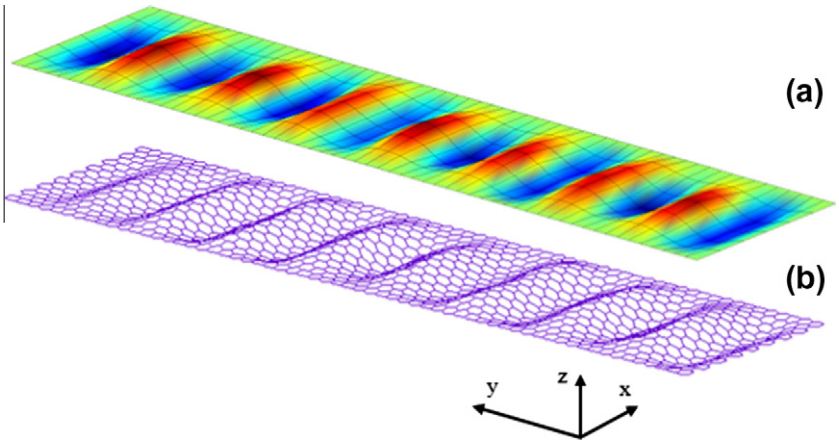

Fig. 2. Snapshots of wave propagation in a GS with a width of 3.62 nm and a length of 15.03 nm subjected to a harmonic deflection of period T = 500 fs at y = 0 with (a) the nonlocal FEM model; (b) MD simulations.

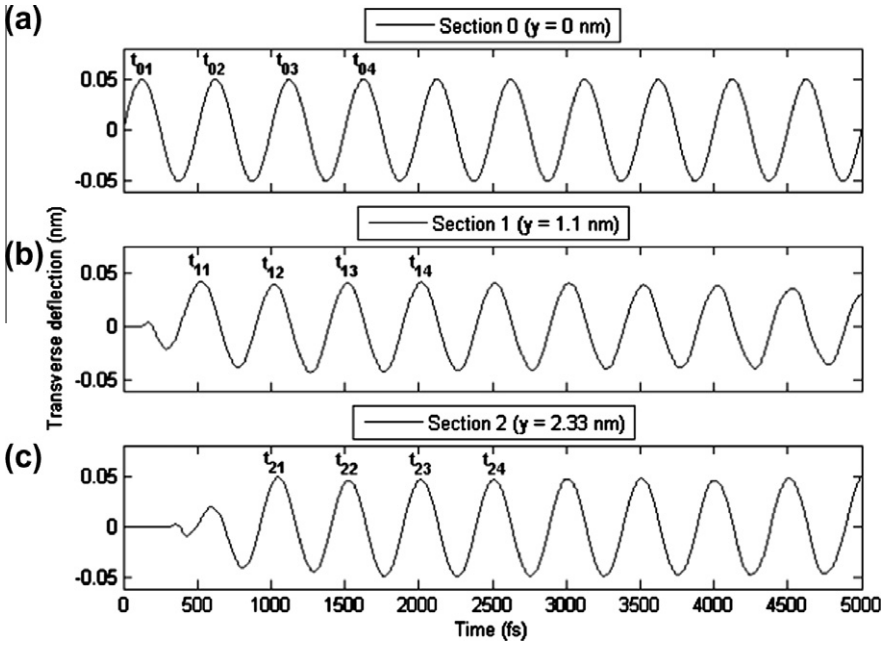

Fig. 3. Time histories of the deflections of centric atoms at different sections of (a) Section 0 at y = 0; (b) Section 1 at y = 1.1 nm; and (c) Section 2 at y = 2.33 nm in a GS with a size of 3.62 × 15.03 nm subjected to a harmonic deflection of period T = 500 fs at y = 0.

and (c) provide the transverse vibrations of the centric atoms in Section 1 at y = 1.1 nm and Section 2 at y = 2.33 nm, respectively. The transient deflections of the first two periods are neglected to remove the effect of initial uncertainties on the velocity measurements, and the propagation duration Δt of the wave from Sections 1 and 2 can be estimated as [28]

$$\Delta t \approx \frac{(t_{23}-t_{13})+(t_{24}-t_{14})+\cdots+(t_{2n}-t_{1n})}{n-2}, \tag{15}$$

where subscripts i and j in t_{ij} represent the number of the sections and the number of the wave peaks, respectively. The phase velocity and wavenumber are thus respectively obtained to be,

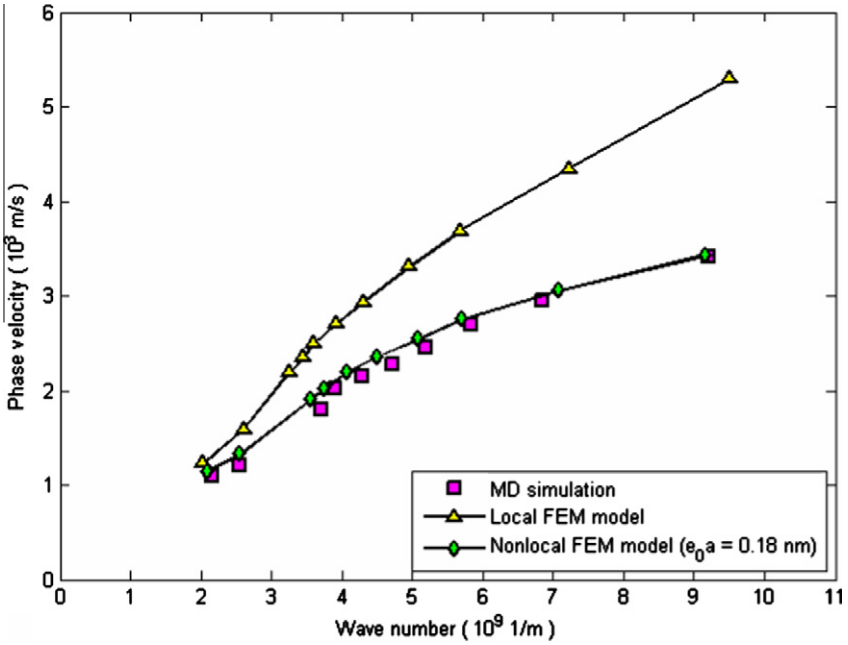

Fig. 4. Dispersion relations of a GS with a size of 3.62 nm × 15.03 nm obtained from MD simulations, the local FEM plate model, and the nonlocal FEM model.

$$c = \frac{y_2 - y_1}{\Delta t}, \quad k = \frac{2\pi}{\lambda} = \frac{\omega T}{\lambda} = \frac{\omega}{c}, \tag{16}$$

where λ is the wavelength. From Eq. (16) the phase velocity, c, and the wavenumber, k, of the GS in Figs. 2 and 3 are respectively obtained to be 2.42×10^3 m/s and 5.19×10^9 l/m by MD simulations. We also did simulations to see the effect of chirality on the wave solution. The simulation results show the phase velocity, c, and the wavenumber, k, of a zigzag GS with a size of 3.69 × 15.12 nm, that is similar to the size studied in Figs. 2 and 3, are 2.39×10^3 m/s and 5.22×10^9 l/m, respectively. The finding reveals that chirality of graphene sheets has very small effect on the dispersion relations. The observation also reported in Ref. [34].

Fig. 4 illustrates the dispersion relations, i.e. the relation between the phase velocity and the wavenumber, of the transverse wave in the GS from MD simulations, local and nonlocal FE plate models. The value of the nonlocal parameter e_0a has been calibrated based on a nonlinear least-square fitting procedure by minimizing the Euclidean norm of the difference between the phase velocies obtained directly from the MD simulations and the ones calculated by the nonlocal elastic plate model. It is recommended a calibrated nonlocal parameter e_0a = 0.18 nm is adopted for wave propagation in the GS with the nonlocal elastic plate model for wavenumber ranging from 2.55×10^9 to 9.17×10^9 l/m. From Fig. 4, it is found that as wavenumber increases from 2.55×10^9 to 9.17×10^9 l/m, the phase velocity tends to increase from 1.32×10^3 to 3.44×10^3 m/s and the small length scale effects become dominant indicating a high scale effect in wave propagation in the GS. The amounts of overestimation of the phase velocity predicted by the local plate model, compared to MD simulations and the nonlocal theory, are almost 30% at the wavenumber of $5.83 \times 10^9$1/m or the wavelength of 1.08 nm, and 37% at the wavenumber of $9.17 \times 10^9$1/m or the wavelength of 0.68 nm. It is concluded that the nonlocal FE model is indispensable for an accurate estimate of the wave dispersion relations when the wavelength is approximately less than 1 nm. On the other hand, the maximum percentage difference between the phase velocity obtained from MD simulation and the nonlocal FEM plate model with a nonlocal parameter of e_0a = 0.18 nm is only 6% at wave number of 3.71×10^9 l/m shown by the phase velocity obtained from MD simulation and the nonlocal being respectively 1.69×10^3 and 1.81×10^3 m/s. The percentage difference decreases to up to 3% and 1.3% at wave number of 5.19×10^9 and 6.85×10^9 l/m. The simulation results show that an unique calibrated value of the nonlocal parameter, e_0a = 0.18 nm, can be used for a relatively wide range of wave number ranging from 2.55×10^9 to 9.17×10^9 l/m.

Fig. 4 also shows that the overestimation of the phase velocity predicted by the local plate model, compared to MD simulations and the nonlocal theory, decreases to only 3% at the wavenumber of 2.03×10^9 l/m or the wavelength of 3.09 nm. It can thus be concluded that the small-scale effect is almost negligible at wavelength of 3 nm, above which the wave solution predicted by the local plate model converge to that by the nonlocal continuum model.

To decrease the ripple effect on wave propagation, the two edges of the GS are fixed in the width direction. To investigate the size effect of the width of a GS on wave dispersion in the GS, the variation of the phase velocity in a GS with a length of 15.03 nm subjected to a harmonic deflection of period T = 500 fs versus its width ranging from 2.34 to 12.14 nm is plotted in Fig. 5. The results based on the nonlocal model with the calibrated nonlocal parameter of 0.18 nm are in very good agreement with those obtained by MD simulations. The comparison of MD simulations and the nonlcoal FE model results also shows that the nonlocal parameter is insensitive to the size of GSs. It is seen that the phase velocity obtained by MD simulations and nonlocal FE model decreases from 2.46×10^3 to 2.35×10^3 m/s with an increase in the width of the GS from 2.34 to 12.14 nm, and the decrease slows down at widths larger than 9 nm to an asymptotic phase velocity of 2.35×10^3 m/s. The asymptotic value obtained by nonlocal analytical model is exactly in agreement with that obtained from the theoretical elastic plate model presented in Eq. (6). It also reveals that the effect of boundary conditions of GSs decreases with an increase in the width size of GSs.

In the following simulations, the potential of GSs as nano-sensors in detection of distinct gas atoms on its surface is examined via a wave propagation analysis. The sensor takes advantage of

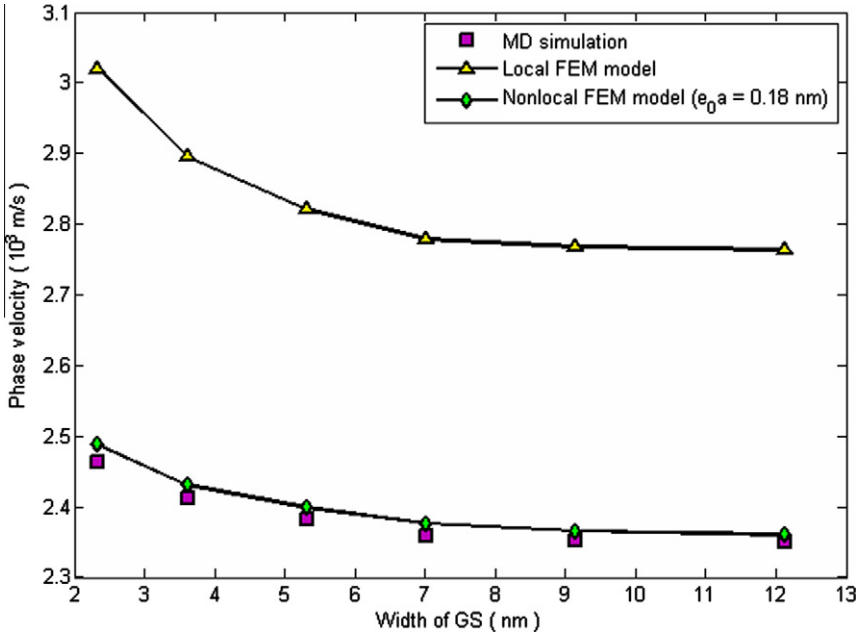

Fig. 5. Variation of the phase velocity versus the width of a GS with a length of 15.03 nm subjected to a harmonic deflection of period $T = 500$ fs at $y = 0$.

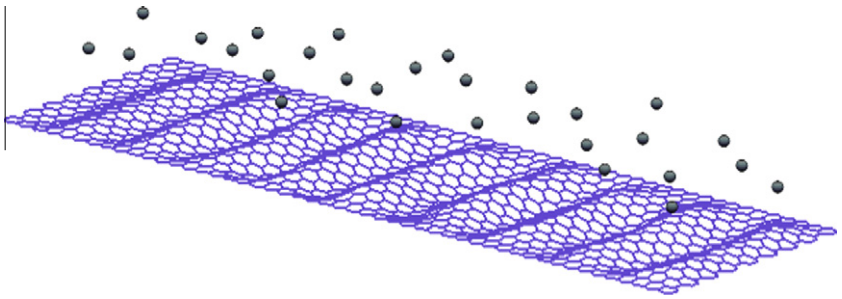

Fig. 6. Snapshot of wave propagation in a GS with a size of 3.62×15.03 nm and attached by 30 Xe atoms on its surface subjected to a harmonic deflection of period $T = 500$ fs at $y = 0$.

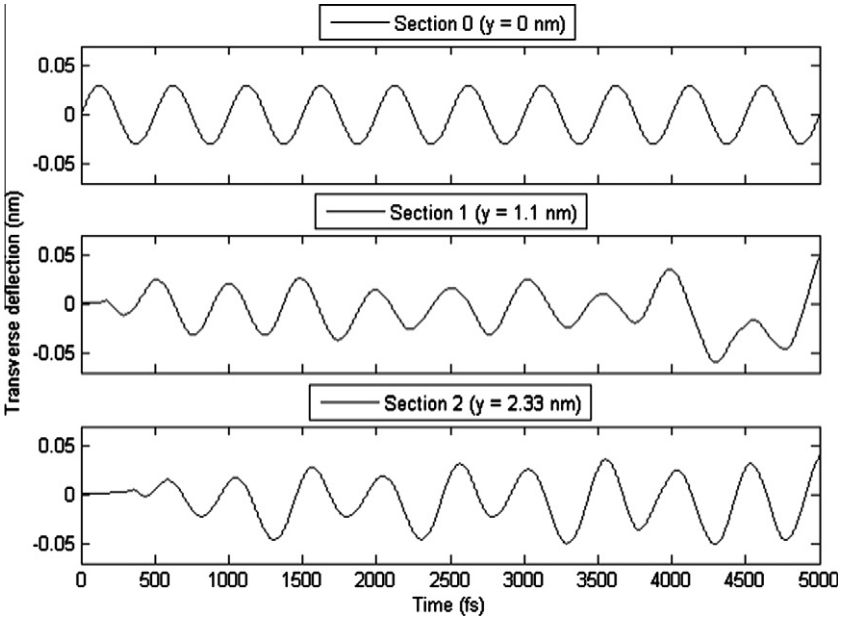

Fig. 7. Time histories of the deflection of centric atoms at Section 0 at $y = 0$, Section 1 at $y = 1.1$ nm, and Section 2 at $y = 2.33$ nm respectively in a GS with a size of 3.62×15.03 nm subjected to a harmonic deflection of period $T = 500$ fs at $y = 0$ and attached by 30 Xe atoms on its surface.

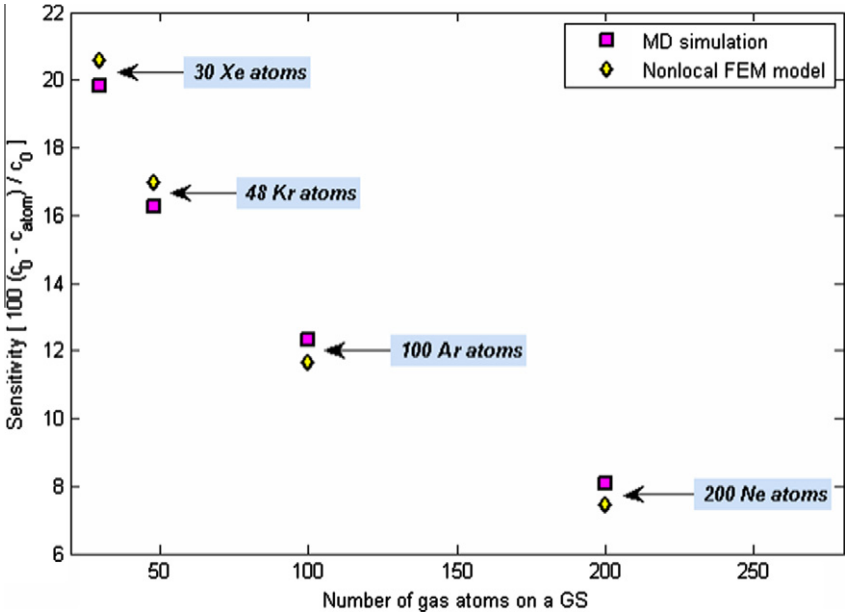

Fig. 8. The sensitivity of a GS with a size of 3.62 nm × 15.03 nm subjected to a harmonic deflection of period $T = 500$ fs and attached by 30 Xe, 48 Kr, 100 Ar and 200 Ne atoms respectively (around 6.7 fg for each type of atoms) on its surface.

the phase velocity shift in a GS by gas atoms on its surface and an index representing the sensitivity of the possible graphene sensor is defined to be $100\frac{c_0-c_{atom}}{c_0}$. In the definition, c_{atoms} and c_0 are respectively the phase velocity in the GS with and without gas atoms on its surface. The advantage of the present method is that only wave peaks of two arbitrary sections of the GS are recorded to calculate wave velocity, while in previous studies based on the vibration analysis [11], trajectories of atoms in a period of time are required to estimate resonant frequency by using the fast Fourier transform. Thus, less sensor information is necessary in present the method which may enhance the applicability of GSs as nano-sensors in experiments.

Fig. 6 presents a snapshot of the GS studied in Figs. 2–4 attached by 30 Xe atoms on its surface during wave propagation subjected to a harmonic deflection of period $T = 500$ fs at $y = 0$. Time history of centric atoms in Section 0 at $y = 0$, Section 1 at $y = 1.1$ nm and Section 2 at $y = 2.33$ nm of the GS is provided in Fig. 7. From Fig. 7, the phase velocity in the GS is obtained to be 1.941×10^3 m/s by MD simulations revealing a decrease of 19.82% in the phase velocity compared to that of a pristine GS shown in Fig. 3.

The findings can be interpreted by using the explicit wave dispersion relation presented in Eq. (6). The mass density of a pristine GS and GS attached by gas atoms is respectively assumed ρ and $\rho_{mass} = \rho + \frac{M_{atoms}}{Ah}$ showing an increase in the mass density as high as $\frac{M_{atoms}}{Ah}$ where M_{atoms}, A and h are total mass of gas atoms on the GS, area of the GS and the effective thickness of the GS. From Eq. (6), it can be concluded that the phase velocity should decrease by an increase in the mass density which physically justifies results obtained by MD simulations in Fig 7. It is noteworthy that the continuum model derived by the theoretical elastic plate model cannot be directly used here because distribution of gas atoms on the GS and clamped boundary condition to make the GS stiffer cannot be considered in the simple model, and hence the nonlocal FE model is employed to compromise the limitations by the theoretical model.

Fig. 8 shows the applicability of graphenes as nano-sensors in detecting distinct gas atoms. In the following simulations, the sensitivity index is employed to differentiate distinct gases with the same mass. The sensitivity of the GS sensor illustrated in Figs. 6 and 7 attached by 30 Xe, 48 Kr, 100 Ar and 200 Ne atoms with a mass of around 6.7 fg, for each type of atoms, on its surface is shown in Fig. 8. It is obvious that there is a distinct region of the mass sensitivity for each type of the attached atoms. The mass sensitivity indexes are found to be around 20% 16%, 12% and 8% for Xe, Kr, Ar and Ne atoms in MD simulations, respectively. Moreover, the nonlocal FE plate model provides an accurate estimation compared to MD simulations with a variation less than 1%. For example, the sensitivity of the GS attached by 30 Xe atoms predicted by MD simulations and the nonlocal FE model are 19.82% and 20.59%, respectively. The sensitivity is found to be decreased when lighter atoms that are distributed more uniformly is to be detected. These findings confirm the applicability of the GS-based sensors in detecting distinct of gases on the graphenes with the model proposed in the current study on wave propagations in GSs.

5. Conclusions

A study of the transverse wave propagation in GSs is presented by use of the nonlocal FE plate model and MD simulations. The results based on the nonlocal model are in good agreement with those obtained by MD simulations. The classical continuum model tends to overestimate the wave dispersion relations of a GS, especially for small wavelengths. It is found that the nonlocal FE model is indispensable in analysis of GSs when the wavelength is approximately less than 1 nm. The effect of the GS width size on the wave dispersion is studied and the simulation results indicate that the phase velocity leads to an asymptotic value with an increase in sheet width. The value of the nonlocal parameter e_0a is calibrated based on the MD results.

The potential of a GS as a nano-sensor is explored. The wave propagation in a graphene sheet with various noble gas atoms on its surface is simulated by MD simulations and the nonlocal FE model for a mass detection purpose. In simulations of a GS with a size of 3.62 × 15.03 nm attached by gas atoms about 6.7 fg randomly placed on the sensor, it is found that distinct noble gas atoms are successfully differentiated by identifying a recognizable sensitivity.

Acknowledgements

This research was undertaken, in part, thanks to funding from the Canada Research Chairs Program (CRC) and the National Science and Engineering Research Council (NSERC). The work described in this paper was also supported by Grants from the Research Grants Council of the Hong Kong Special Administrative Region, China (Project No. 9041674, CityU 118411) and the China National Natural Science Foundation (Grant No. 11172253).

References

[1] K.S. Novoselov, A.K. Geim, S.V. Morozov, D. Jiang, Y. Zhang, S.V. Dubonos, I.V. Grigorieva, A.A. Firsov, Electric field effect in atomically thin carbon films, Science 306 (2004) 666–669.
[2] T. Ohta, A. Bostwick, T. Seyller, K. Horn, E. Rotenberg, Controlling the electronic structure of bilayer graphene, Science 313 (2006) 951–954.
[3] C. Lee, X. Wei, J.W. Kysar, J. Hone, Measurement of the elastic properties and intrinsic strength of monolayer graphene, Science 321 (2008) 385–388.
[4] J.H. Seol, I. Jo, A.L. Moore, L. Lindsay, Z.H. Aitken, M.T. Pettes, X. Li, Z. Yao, R. Huang, D. Broido, N. Mingo, R.S. Ruoff, L. Shi, Two-dimensional phonon transport in supported graphene, Science 328 (2010) 213–216.
[5] F. Schedin, A.K. Geim, S.V. Morozov, E.W. Hill, P. Blake, M.I. Katsnelson, K.S. Novoselov, Detection of individual gas molecules adsorbed on graphene, Nat. Mater. 6 (2007) 652–655.
[6] J.S. Bunch, A.M. van der Zande, S.S. Verbridge, I.W. Frank, D.M. Tanenbaum, J.M. Parpia, H.G. Craighead, P.L. McEuen, Electromechanical resonators from graphene sheets, Science 315 (2007) 490–493.
[7] S. Stankovich, D.A. Dikin, G.H.B. Dommett, K.M. Kohlhaas, E.J. Zimney, E.A. Stach, R.D. Piner, S.T. Nguyen, R.S. Ruoff, Graphene-based composite materials, Nature 442 (2006) 282–286.
[8] R. Chowdhury, S. Adhikari, P. Rees, S.P. Wilks, Graphene-based biosensor using transport properties, Phys. Rev. B 83 (2011) 045401.
[9] C. Sirtori, Applied physics: bridge for the terahertz gap nature 417 (2002) 132–133.
[10] M. Chen, J. Zang, D. Xiao, C. Zhang, F. Liu, Nanopumping molecules via a carbon nanotube, Nano Res. 2 (2009) 938–944.
[11] Y.Z. He, H. Li, P.C. Si, Y.F. Li, H.Q. Yu, X.Q. Zhang, F. Ding, K.M. Liew, X.F. Liu, Dynamic ripples in single layer grapheme, Appl. Phys. Lett. 98 (2011) 063101.
[12] B. Arash, Q. Wang, W.H. Duan, Detection of gas atoms via vibration of graphenes, Phys. Lett. A 375 (2011) 2411–2415.
[13] S. Iijima, C. Brabec, A. Maiti, J. Bernholc, Structural flexibility of carbon nanotubes, J. Chem. Phys. 104 (1996) 2089–2092.
[14] E. Hernandez, C. Goze, P. Bernier, A. Rubio, Elastic properties of C and BxCyNz composite nanotubes, Phys. Rev. Lett. 80 (1998) 4502–4505.
[15] D. Sanchez-Porta, E. Artacho, J.M. Soler, A. Rubio, P. Ordejon, Ab initio structural, elastic, and vibrational properties of carbon nanotubes, Phys. Rev. B 59 (1999) 12678–12688.
[16] R. Chowdhury, S. Adhikari, F. Scarpa, M.I. Friswell, Transverse vibration of single-layer graphene sheets, J. Phys. D Appl. Phys. 44 (2011) 205401.
[17] R. Khare, S.L. Mielke, G.C. Schatz, T. Belytschko, Multiscale coupling schemes spanning the quantum mechanical, atomistic forcefield, and continuum regimes, Comput. Method Appl. M. 197 (2008) 3190–3202.
[18] D. Qian, W.K. Liu, Q. Zheng, Concurrent quantum/continuum coupling analysis of nanostructures, Comput. Method Appl. M. 197 (2008) 3291–3323.
[19] B.I. Yakobson, C.J. Brabec, J. Bernholc, Nanomechanics of carbon tubes: instabilities beyond linear response, Phys. Rev. Lett. 76 (1996) 2511–2514.
[20] A. Krishnan, E. Dujardin, T.W. Ebbesen, P.N. Yianilos, M.M.J. Treacy, Young's modulus of single-walled nanotubes, Phys. Rev. B 58 (1998) 14013–14019.
[21] Y. Chandra, R. Chowdhury, F. Scarpa, S. Adhikaricor, Vibrational characteristics of bilayer graphene sheets, Thin Solid Films 519 (2011) 6026–6032.
[22] Q. Wang, V.K. Varadan, S.T. Quek, Small scale effect on elastic buckling of carbon nanotubes with nonlocal continuum models, Phys. Lett. A 357 (2006) 130–135.
[23] K.M. Liew, Q. Wang, Analysis of wave propagation in carbon nanotubes via elastic shell theories, Int. J. Eng. Sci. 45 (2007) 227–241.
[24] B. Arash, Q. Wang, Vibration of single- and double-layered graphene sheets, J. Nanotechnol. Eng. Med. 2 (2011) 011012.
[25] A.C. Eringen, Nonlocal Polar Field Models, Springer, Berlin, 1976.
[26] A.C. Eringen, On differential equations of nonlocal elasticity and solutions of screw dislocation and surface waves, J. Appl. Phys. 54 (1983) 4703.
[27] Q. Wang, Wave propagation in carbon nanotubes via nonlocal continuum mechanics, J. Appl. Phys. 98 (2005) 124301.
[28] L. Wang, H. Hu, Flexural wave propagation in single-walled carbon nanotubes, Phys. Rev. B 71 (2005) 195412.
[29] Q. Wang, V.K. Varadan, Application of nonlocal elastic shell theory in wave propagation analysis of carbon nanotubes, Smart Mater. Struct. 16 (2007) 178–190.
[30] Y.G. Hu, K.M. Liew, Q. Wang, X.Q. He, B.I. Yakobson, Nonlocal shell model for elastic wave propagation in single- and double-walled carbon nanotubes, J. Mech. Phys. Solids 56 (2008) 3475–3485.
[31] Y.Z. Wang, F.M. Li, K. Kishimoto, Scale effects on the longitudinal wave propagation in nanoplates, Physica E 42 (2010) 1311–1317.
[32] S. Narendar, D.R. Mahapatra, S. Gopalakrishnan, Investigation of the effect of nonlocal scale on ultrasonic wave dispersion characteristics of a monolayer graphene, Comp. Mater. Sci. 49 (2010) 734–742.
[33] P. Thalmeier, B. Dóra, K. Ziegler, Surface acoustic wave propagation in graphene, Phys. Rev. B 81 (2010) 041409.
[34] S.Y. Kim, H.S. Park, On the effective plate thickness of monolayer graphene from flexural wave propagation, J. Appl. Phys. 110 (2011) 054324.
[35] F. Scarpa, R. Chowdhury, Kenneth Kam, S. Adhikari, M. Ruzzene, Dynamics of mechanical waves in periodic graphene nanoribbon assemblies, Nanoscale Res. Lett. 6 (2011) 430.
[36] W.H. Duan, K. Gong, Q. Wang, Controlling the formation of wrinkles in a single layer graphene sheet subjected to in-plane shear, Carbon 49 (2011) 3107–3112.
[37] O.O. Ochoa, J.N. Reddy, Finite Element Analysis of Composite Laminates, Springer, 1992.
[38] K.-J. Bathe, Finite Element Procedures, Prentice Hall, 1996.
[39] D.W. Brenner, O.A. Shenderova, J.A. Harrison, S.J. Stuart, B. Ni, S.B. Sinnott, A second-generation reactive empirical bond order (REBO) potential energy expression for hydrocarbons, J. Phys. Condens. Matter 14 (2002) 783–802.
[40] J.E. Jones, On the determination of molecular fields. I. From the variation of the viscosity of a gas with temperature, Proc. R. Soc. Lond. A 106 (1924) 441–462.
[41] M.P. Allen, D.J. Tildesley, Computer Simulation of Liquids, Oxford University Press, 1989.
[42] W.G. Hoover, Canonical dynamics: equilibrium phase-space distributions, Phys. Rev. A 31 (1985) 1695–1697.
[43] Q. Wang, K.M. Liew, Molecular mechanics modeling for properties of carbon nanotubes, J. Appl. Phys. 103 (2008) 046103.